

A MECHANISM FOR THE DEPENDENCE OF SUNSPOT GROUP TILT ANGLES ON CYCLE STRENGTH

EMRE IŞIK^{1,2}

¹ Department of Physics, Faculty of Science and Letters, İstanbul Kültür University, 34156, Bakırköy, İstanbul, Turkey

² Feza Gürsey Center for Physics and Mathematics, Boğaziçi University, 34684, Çengelköy, İstanbul, Turkey

Draft version October 28, 2015

ABSTRACT

The average tilt angle of sunspot groups emerging throughout the solar cycle determines the net magnetic flux crossing the equator, which is correlated with the strength of the subsequent cycle. I suggest that a deep-seated, non-local process can account for the observed cycle-dependent changes in the average tilt angle. Motivated by helioseismic observations indicating cycle-scale variations in the sound speed near the base of the convection zone, I determined the effect of a thermally perturbed overshoot region on the stability of flux tubes and on the tilt angles of emerging flux loops. I found that 5-20 K of cooling is sufficient for emerging flux loops to reproduce the reported amplitude of cycle-averaged tilt angle variations, suggesting that it is a plausible effect responsible for the nonlinearity of the solar activity cycle.

Keywords: Sun: activity — Sun: interior — Sun: magnetic fields — sunspots

1. INTRODUCTION

One of the unsolved problems of the solar activity cycle is the physical nature of the mechanism(s) underlying the observed variations in cycle amplitude (Charbonneau 2010). Among several possibilities, reduction of poloidal flux generation by reducing the average tilt angle of bipolar magnetic regions has recently been considered as a plausible candidate. Analysis of tilt angle data from Mt. Wilson and Kodaikanal observatories between solar cycles 15-21 by Dasi-Espuig et al. (2010) has led to the discovery that the cycle-averaged sunspot group tilt angle was inversely correlated with the cycle strength. In terms of the Babcock-Leighton dynamo process, this means that the surface source for the poloidal field becomes weaker for stronger cycles, potentially limiting the strength of the next cycle.

A possible explanation for the observed anti-correlation is based on the effective reduction of the tilt angle by inflows toward activity belts, which are observed by local helioseismic techniques (González Hernández et al. 2008). Incorporation of such inflows into surface flux transport models has shown the efficiency of this mechanism in limiting the solar axial dipole moment (Jiang et al. 2010; Cameron et al. 2010; Cameron & Schüssler 2012).

As already discussed by Dasi-Espuig et al. (2010), systematic changes in the tilt angle can also be led by changes in the internal structure of the lower convection zone, a potential location for the origin of magnetic flux loops which produce sunspot groups. An observational hint came from global helioseismology of low-degree oscillation modes by Baldner & Basu (2008), who found a statistically significant reduction in the acoustic wave speed near the base of the convection zone between the minimum and maximum of cycle 23. A temperature perturbation mainly in the same direction (cooling) was predicted by Rempel (2003), who considered a magnetic layer near the base of the convection zone and obtained time-dependent solutions for radial heat transport by in-

cluding radiative heating from below, in the presence of an imposed horizontal magnetic field reaching 10^5 G.

In addition to radiative effects on stratification, stronger cycles possibly involve more frequent flux tube explosions in the midst of the convection zone (Moreno-Insertis et al. 1995; Rempel & Schüssler 2001; Hotta et al. 2012). This can also lead to a decrease in the radial entropy gradient, hence a decrease in the (negative) superadiabaticity in the lower convection zone.

In both the convection quenching and the entropy mixing scenarios, the convection zone would be increasingly stabilized for stronger magnetic fields. Consequently, the critical field strength for the onset of flux tube instability would be raised with the cycle strength. Flux tubes would then become unstable at higher field strengths, emerge at the surface with smaller tilt angles owing to stronger tension force.

Motivated by the helioseismic observations and the theoretical arguments summarized above, I determine the variation in the thermal perturbation required to account for the observed changes in the cycle-averaged tilt angle. The results indicate that a thermodynamic cycle in phase with the activity cycle at the base of the convection zone can be responsible for the nonlinear saturation of the solar dynamo.

2. THE MODEL

I use a one-dimensional stratification model of the solar convection zone (Skaley & Stix 1991), which uses the non-local mixing length formalism of Shaviv & Salpeter (1973). This model allows for a weakly subadiabatic lower convection zone below $0.775R_{\odot}$, extending down to where the convective heat flux changes sign at about $0.736R_{\odot}$. The convective overshoot region extends from this location down to $0.721R_{\odot}$, with a thickness of about 10^4 km.

2.1. Perturbations to the stratification

To approximate the effect of radiative heating of a magnetic layer in the overshoot region as estimated by Rempel (2003), I model the change in the stratification sim-

ply as a decrease in the temperature with an asymmetric piecewise Gaussian perturbation of the form

$$T_1 = T_m \exp \left[\frac{-(r - r_p)^2}{\sigma_{\pm}^2} \right], \quad (1)$$

where T_m is the amplitude of the perturbation, centered at $r_p = 5 \times 10^{10}$ cm ($0.718R_{\odot}$), and σ_{\pm} is the characteristic width of the distribution, with $\sigma_- = 400$ km for $r < r_p$, and $\sigma_+ = 4000$ km for $r \geq r_p$. Denoting the background thermodynamic variables by index 0 and the perturbations by index 1, I assume that the perturbations satisfy hydrostatic equilibrium,

$$\frac{dp_1}{dr} = -\rho_1 g. \quad (2)$$

For linear perturbations the ideal gas relation takes the form

$$\rho_1 = \rho_0 \left(\frac{p_1}{p_0} - \frac{T_1}{T_0} \right). \quad (3)$$

Using Eq. (3) in Eq. (2), I obtain

$$\frac{dp_1}{dr} = -\frac{p_1}{H_{p0}} + \rho_0 g \frac{T_1}{T_0}, \quad (4)$$

where $H_{p0}(r) := p_0/(\rho_0 g)$ is the pressure scale height in the unperturbed stratification. For simplicity, I assume that flux tubes leading to sunspot groups have a sufficiently low filling factor within a diffuse background field, so that the contribution of magnetic pressure to the hydrostatic equilibrium is neglected against the other terms in Eq. (4).

The perturbation in specific entropy, s_1 , can be determined by writing energy conservation in the thermodynamic notation

$$s_1 \equiv ds = \frac{1}{T} [du + pd(\rho^{-1})], \quad (5)$$

where u is the internal energy. Writing du and $d\rho$ in terms of dT and dp and expressing the differential quantities as perturbations leads to

$$s_1 = c_p \left(\frac{T_1}{T_0} - \nabla_{\text{ad}} \frac{p_1}{p_0} \right), \quad (6)$$

where $\nabla_{\text{ad}} := (\partial \ln T_0 / \partial \ln p_0)_s = 1 - \gamma^{-1}$ is the adiabatic temperature gradient.

The most critical quantity which determines the mechanical stability of magnetic flux tubes in the overshoot region is the superadiabaticity $\delta := \nabla - \nabla_{\text{ad}}$, whose perturbation reads

$$\delta_1 = -\frac{H_{p0}}{c_p} \frac{ds_1}{dr}. \quad (7)$$

Using Eqs. (3), (6), and (7), the perturbation in the superadiabaticity is found to be

$$\delta_1 = H_{p0} \left(\frac{1}{\rho_0} \frac{d\rho_1}{dr} - \frac{1}{\gamma p_0} \frac{dp_1}{dr} - \frac{\rho_1}{\rho_0^2} \frac{d\rho_0}{dr} + \frac{p_1}{\gamma p_0^2} \frac{dp_0}{dr} \right). \quad (8)$$

2.2. Linear stability of magnetic flux tubes

To determine the effects of the modified stratification on rising flux tubes, I first calculate the conditions for

the linear stability of flux tubes in the overshoot region, following the procedure described by Ferriz-Mas & Schüssler (1995), in which linear perturbations are applied on a toroidal flux ring in mechanical equilibrium and in spherical geometry, using the thin flux tube approximation. As a function of the radial location, latitude, and field strength of the flux ring, the fastest-growing azimuthal wave mode is obtained from the real parts of the complex roots of the dispersion relation, in the unstable regime, for a set of p , ρ , g , δ , H_p , and Ω , the angular rotation speed. Differential rotation has been taken into account, also for Section 2.3, using an internal rotation profile $\Omega(r, \theta)$ (Işık et al. 2011, Eq. 23) representing helioseismic inversions (Schou et al. 1998).

2.3. Nonlinear dynamics of magnetic flux tubes

To simulate the nonlinear evolution of flux tubes, I use a code developed by Moreno-Insertis (1986) and extended to 3D spherical geometry in the Lagrangian frame by Caligari et al. (1995). The code solves the fluid equations in ideal MHD, taking into account the hydrodynamic drag force and assuming isentropic evolution for the flux tube. The thermodynamic quantities corresponding to the radial location of each mass element of the tube are determined from the stratification model described above, which has 3000 grid points over an adaptive mesh, spanning from $0.56R_{\odot}$ to the surface. The flux tube itself has periodic boundaries and 1000 mass elements.

Initially a flux ring is taken to be in mechanical equilibrium, which is set by neutral buoyancy and a prograde azimuthal flow, which balances the magnetic curvature force in the rotating frame. Azimuthally periodic perturbations are applied, in the form of a linear combination of modes with azimuthal wavenumbers from $m = 1$ to $m = 5$, with amplitudes of the order of $10^{-5}H_p$. For unstable, rising flux tubes, the simulations stop when the top portion of the tube expands to the extent that the thin flux tube approximation becomes inapplicable, *i.e.*, when the cross-sectional radius of the tube exceeds $2H_p$. This occurs at a height of about $0.98R_{\odot}$. To measure the tilt angles, the latitudinal and longitudinal distances between the preceding and follower legs of emerging flux loops are obtained at the same depth ($0.97R_{\odot}$).

3. RESULTS

3.1. Effects on stratification

I now solve Eq. (4) numerically, using a fourth-order Runge-Kutta scheme, by taking the equilibrium quantities as a function of radius from the stratification model, and the corresponding perturbations from Eqs. (1-8). The radial profile of the pressure perturbation is then obtained by setting $p_1 = 0$ at $r = 0.56R_{\odot}$ as the initial value. The radial profiles of the perturbations T_1 , p_1 , ρ_1 , and δ_1 are shown in Fig. 1, for $T_m = -50$ K. Despite the simplifications made in Section 2.1, the resulting profile of δ_1 has a similar shape and amplitude to the result of Rempel (2003).

The profile δ_1 of Fig. 1d is shown in more detail in Fig. 2, along with the unperturbed $|\delta|$ profile. The effect of the thermal perturbation is such that the stratification is destabilized within a narrow layer in the radiative zone, though its relative effect on the highly subadiabatic

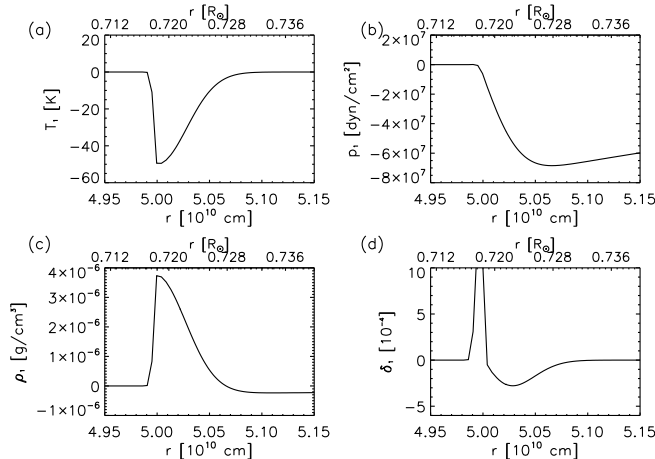


Figure 1. Radial profiles of first-order perturbations in (a) temperature, (b) gas pressure, (c) gas density, and (d) superadiabaticity, as a function of solar radius.

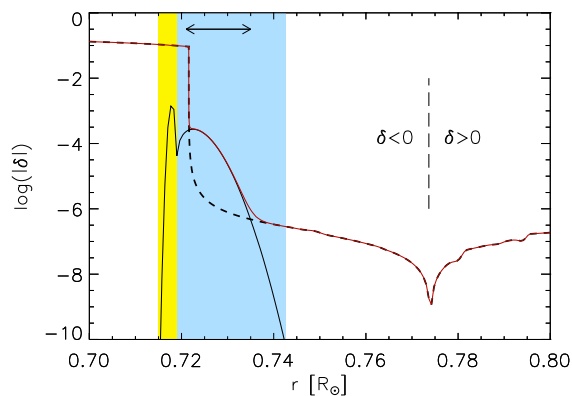


Figure 2. Radial profile the absolute superadiabaticity, $|\delta|$. The dashed curve shows the unperturbed profile, $|\delta_0|$, with the transition between the subadiabatic and superadiabatic regions marked by the long-dashed vertical line. The solid black line shows the perturbation $|\delta_1|$, and the red curve shows $|\delta_0 + \delta_1|$. The double arrow shows the extent of the overshoot region. In the yellow- and blue-shaded regions the perturbation is positive and negative, respectively.

environment is insignificant (the yellow region). However, in the blue-shaded region between about $0.72R_\odot$ and $0.74R_\odot$, the stratification is considerably stabilized, mainly in the overshoot region (arrowed line).

3.2. Instability of flux tubes

How would the modified stratification affect the mechanical stability of magnetic flux tubes in the convective overshoot region? I first calculate the influence of the thermal perturbation (Section 2.1) on the linear instability map of thin toroidal flux tubes subject to different strengths of thermal perturbation within the layer.

I have set up stratification models corresponding to five values for the amplitude of the temperature perturbation in Eq. (1): $T_m = 0, -5, -10, -20$, and -50 K (labeled T0, T5, T10, T20, and T50). The stability diagrams resulting from the linear stability analysis (Section 2.2) are presented in Fig. 3. As $|T_m|$ is increased, magnetic buoyancy instability sets in at gradually higher field strengths, compared to the unperturbed stratifica-

Table 1
Mean tilt angles and Joy's law parameters.

$T_m (K)$	$\delta (\times 10^{-5})$	$\langle \alpha \rangle$	$\langle \alpha \rangle / \langle \lambda \rangle$	a	γ_0	T
0	-0.098	6.69	0.23	0.25	15.2	1.39
-5	-0.636	5.34	0.21	0.23	13.7	1.22
-10	-1.16	4.29	0.17	0.19	11.2	1.03
-20	-2.24	3.63	0.14	0.15	9.0	0.86
-50	-54.9	2.91	0.11	0.13	7.7	0.72

tion. For T50 (not shown here), flux tubes would have to be 3 to 5 times stronger to become unstable, compared to the unperturbed case, T0.

3.3. Simulating Joy's law

To obtain the average values and latitude dependence of the tilt angle, I have carried out a grid of simulations for all the cases T0–T50, where the initial latitudes and field strengths of the tubes are chosen with 5° intervals in latitude and for linear growth times between 40 and 60 days, with 5-day intervals. The initial location of the flux rings is taken at $0.728R_\odot$, corresponding to the middle of the overshoot region (same as for Fig. 3). The cross-sectional radius of the tube is set to 2000 km, which leads to a magnetic flux of 1.26×10^{22} Mx for a field strength of 10^5 G. The tilt angle as a function of the emergence latitude (Joy's law) is plotted in Fig. 4 for all the cases. To fit the simulation data, I choose the following functions, which are commonly used in observational studies:

$$\alpha(\lambda) = a\lambda, \quad (9)$$

$$\alpha(\lambda) = \gamma_0 \sin \lambda, \quad (10)$$

$$\alpha(\lambda) = T\lambda^{1/2}, \quad (11)$$

where λ is the emergence latitude and α is the tilt angle in degrees, and a , γ_0 , and T are the fit coefficients corresponding to each function. The functions have been fitted using the nonlinear Levenberg-Marquardt algorithm. The form (9) was used by Dasi-Espuig et al. (2010). The sinusoidal function (Eq. 10) was used by Stenflo & Kosovichev (2012). Their data set was based on bipolar magnetic regions from magnetograms, which include plage regions alongside spots, which is the possible reason for their systematically higher tilt angles. The form (11) was used by Cameron et al. (2010) when fitting cycle-dependent tilt angles of Dasi-Espuig et al. (2010), to use in surface flux transport simulations.

Joy's law coefficients resulting from the simulations are given in Table 1, which includes standard and latitude-normalized averages of tilt angles, the fitted parameters for different forms of Joy's law, and also the superadiabaticity at the initial location of the flux tube. The mean tilt angle and Joy's law coefficients are inversely proportional to the amplitude of the thermal perturbation. As a result of the stabilized environment, the tilt angles are systematically lower, owing to increasing magnetic tension between the legs of emerging flux loops. Changing the amplitude of cooling in the middle of the overshoot region from 5 to 20 K roughly accounts for the observed amplitude of cycle-averaged tilt angles for solar cycles 15 to 21. The assumption behind this conclusion is that the average depth from which sunspot region producing flux tubes originate does not change significantly as a function of cycle strength.

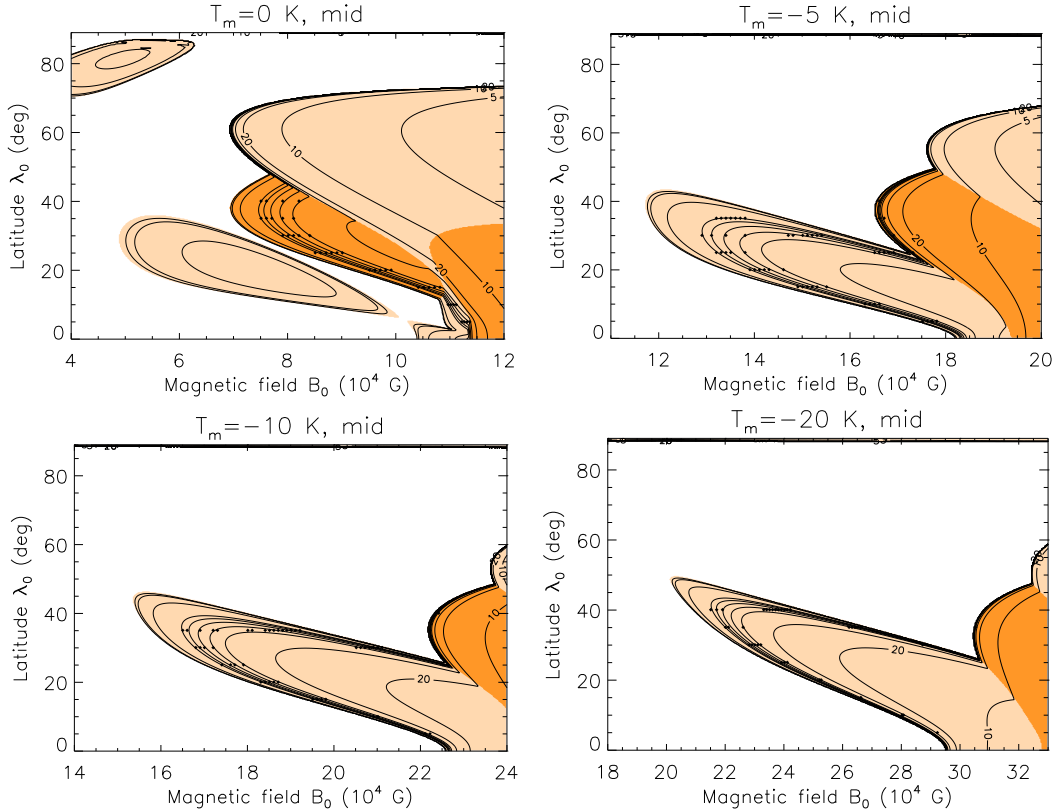


Figure 3. Instability maps of a thin flux tube as a function of latitude and field strength in the middle of the overshoot region, for T0 and T5 (upper panels); T10 and T20 (lower panels). The contours show growth times from the linear stability analysis. The dots clustered along the densely packed contours (growth times 40-60 days with 5-day intervals) show the nonlinear simulations performed. The light (dark) shaded regions denote the wavenumber of the fastest-growing mode $m = 1$ ($m = 2$). It is noticeable that the instability threshold field strength shifts to larger values as the thermal perturbation is increased. Note that the range of field strength is different on each plot.

It should be noted that taking into account the radiative heating of flux tubes has recently been shown to have a mild effect on Joy’s law (higher slopes), in the presence of turbulent convective flow fields (Weber & Fan 2015). In future studies, it would be of interest to include radiative diffusion in flux tube simulations, in conjunction with a cycle-dependent thermal perturbation.

4. COMPARISON WITH HELIOSEISMIC EVIDENCE

The magnitude of the change of sound speed at the base of the convection zone found in the helioseismic analysis of Baldner & Basu (2008) is about $\delta c^2/c^2 = (7.23 \pm 2.08) \times 10^{-5}$, expressed as the difference in the squared sound speed between the solar minimum and maximum, normalized to the minimum value. Assuming that the reduction in wave speed is solely due to a temperature drop, the corresponding cooling amplitude amounts to about -150 ± 45 K. Following the approach taken in Baldner & Basu (2008) and assuming that the change in the sound speed between cycle minimum and maximum is purely due to the change in the local Alfvén speed, an estimate for the magnetic field strength reads from

$$B \simeq \left(4\pi\gamma p \frac{\delta c^2}{c^2} \right)^{1/2}, \quad (12)$$

which is about 3.6×10^5 G, using the sound speed perturbation from the helioseismic result, and the local gas pressure from the structure model used here. From an-

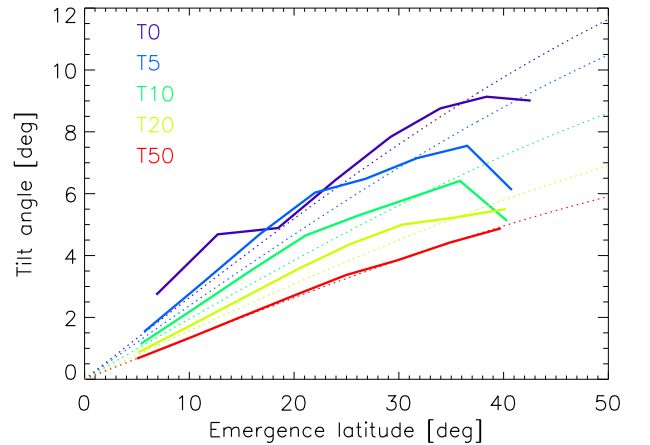


Figure 4. Latitude dependence of the tilt angle (Joy’s law) for simulations T0 to T50 with different amplitudes of local cooling. The tilt angles are averages over 5° bins (continuous lines). The dotted lines show the sinusoidal fits (Eq. 10). The average tilt angle and the steepness of the dependence decrease with increasing temperature perturbation.

other perspective, Rempel (2003) found that when a magnetic field of 10^5 G quenches the convective heat conductivity by a factor of 100, a local cooling of about 40 K would be reached within 6 months, and 50 K within a few years, yielding a profile similar to Fig. 1a. For a quenching factor of 10^4 , he found nearly 200 K within 6

months.

The base location of the convection zone is different in the model used here ($0.736R_{\odot}$) and the helioseismic inversions ($0.713R_{\odot}$, Basu & Antia 1997). However, the instability and eruption properties of flux tubes in the overshoot region are most sensitively determined by the local superadiabaticity. Therefore, when a helioseismically calibrated stratification (e.g., Zhang et al. 2012; Christensen-Dalsgaard et al. 2011) is used, the superadiabaticity values given in Table 1 would lead to similar tilt angles, but the initial depth of flux tubes would be shifted inwards, leading to a similar inverse correlation with the perturbation strength.

In the simulations presented in the previous section, r_p in Eq. (1) has been taken at the radiative zone boundary ($0.718R_{\odot}$), where δ changes very steeply (Fig. 2). I have made this choice to represent the conditions set up in the model of Rempel (2003). However, the central location of the sound speed reduction observed by Baldner & Basu (2008) is at the base of the convection zone, which is at $0.736R_{\odot}$ in the stratification I have used here. Unfortunately, the detailed radial profile or even the extent of the sound speed perturbation cannot be drawn from the helioseismic signal, owing to limited resolution provided by the low frequency waves used to probe the region. Taking r_p at $0.736R_{\odot}$, one finds that T_m on the order of -100 K results in a thin superadiabatic layer, whose thickness is determined by σ_- in Eq. (1), located in the midst of the stably stratified regions. This means either that the stratification where the temperature perturbation occurs would be completely restructured, or that the profile of the sound speed perturbation during solar maximum must have fine structure that could not be detected by Baldner & Basu (2008), possibly involving a region of enhanced sound speed immediately below the reduction region, owing to excess heating from the radiative zone. There are indications of such a layer, though within the upper radiative zone. Owing to such ambiguities, I have not attempted to seek a best fit to the helioseismic and tilt angle measurements in this preliminary study.

5. CONCLUSION

By numerical simulations of thin flux tubes within a thermally perturbed stratification, I have shown that temperature variations of only 5-20 K in the overshoot region among different cycles can reproduce the reported anti-correlation between the tilt angles of sunspot groups and the cycle strength (Dasi-Espuig et al. 2010), provided that the emerging flux loops originate from about the same depth in the overshoot region in different cycles. Thermal fluctuations with such amplitudes among different cycle maxima are possible, because their magnitudes are well below the level of cooling indicated by the sound speed reduction from cycle minimum to maxi-

mum (Baldner & Basu 2008). Whether this is a relevant mechanism for the saturation of the solar dynamo should be tested, through (i) helioseismic observations of sound speed variations at the base of the convection zone for several cycles, in conjunction with (ii) measurements of the cycle-averaged tilt angle of sunspot groups and (iii) theoretical models of the growth of the toroidal magnetic field and its interrelation with the evolving stratification (e.g., Cossette et al. 2013), which would be essential to explain the physics of the possible anti-correlation between the observed tilt angles and the sound speed perturbation.

I am thankful to R. H. Cameron and M. Schüssler for useful discussions which motivated this study. I acknowledge V. R. Holzwarth and Th. Granzer for help with issues related to the stratification model, M. Rempel for valuable comments, C. Sağiroğlu for support with simulations, and the anonymous referee for suggestions that helped to improve the manuscript. This work has been supported by the Scientific and Technological Research Council of Turkey (TÜBİTAK), under project grant 113F070.

REFERENCES

- Baldner, C. S., & Basu, S. 2008, ApJ, 686, 1349
- Basu, S., & Antia, H. M. 1997, MNRAS, 287, 189
- Caligari, P., Moreno-Insertis, F., & Schüssler, M. 1995, ApJ, 441, 886
- Cameron, R. H., Jiang, J., Schmitt, D., & Schüssler, M. 2010, ApJ, 719, 264
- Cameron, R. H., & Schüssler, M. 2012, A&A, 548, A57
- Charbonneau, P. 2010, Living Reviews in Solar Physics, 7, 3
- Christensen-Dalsgaard, J., Monteiro, M. J. P. F. G., Rempel, M., & Thompson, M. J. 2011, MNRAS, 414, 1158
- Cossette, J.-F., Charbonneau, P., & Smolarkiewicz, P. K. 2013, ApJ, 777, L29
- Dasi-Espuig, M., Solanki, S. K., Krivova, N. A., Cameron, R., & Peñuela, T. 2010, A&A, 518, A7
- Ferriz-Mas, A., & Schüssler, M. 1995, Geophysical and Astrophysical Fluid Dynamics, 81, 233
- González Hernández, I., Kholikov, S., Hill, F., Howe, R., & Komm, R. 2008, Sol. Phys., 252, 235
- Hotta, H., Rempel, M., & Yokoyama, T. 2012, ApJ, 759, L24
- Işık, E., Schmitt, D., & Schüssler, M. 2011, A&A, 528, A135
- Jiang, J., Işık, E., Cameron, R. H., Schmitt, D., & Schüssler, M. 2010, ApJ, 717, 597
- Moreno-Insertis, F. 1986, A&A, 166, 291
- Moreno-Insertis, F., Caligari, P., & Schuessler, M. 1995, ApJ, 452, 894
- Rempel, M. 2003, A&A, 397, 1097
- Rempel, M., & Schüssler, M. 2001, ApJ, 552, L171
- Schou, J., Antia, H. M., Basu, S., et al. 1998, ApJ, 505, 390
- Shaviv, G., & Salpeter, E. E. 1973, ApJ, 184, 191
- Skaley, D., & Stix, M. 1991, A&A, 241, 227
- Stenflo, J. O., & Kosovichev, A. G. 2012, ApJ, 745, 129
- Weber, M. A., & Fan, Y. 2015, Sol. Phys., 290, 1295
- Zhang, C., Deng, L., Xiong, D., & Christensen-Dalsgaard, J. 2012, ApJ, 759, L14